



This is a repository copy of *Nanoscale wafer patterning using SPM induced local anodic oxidation in InP substrates*.

White Rose Research Online URL for this paper:
<https://eprints.whiterose.ac.uk/182271/>

Version: Published Version

Article:

Ovenden, C., Farrer, I. orcid.org/0000-0002-3033-4306, Skolnick, M.S. et al. (1 more author) (2022) Nanoscale wafer patterning using SPM induced local anodic oxidation in InP substrates. *Semiconductor Science and Technology*, 37 (2). 025001. ISSN 0268-1242

<https://doi.org/10.1088/1361-6641/ac3f20>

Reuse

This article is distributed under the terms of the Creative Commons Attribution (CC BY) licence. This licence allows you to distribute, remix, tweak, and build upon the work, even commercially, as long as you credit the authors for the original work. More information and the full terms of the licence here:
<https://creativecommons.org/licenses/>

Takedown

If you consider content in White Rose Research Online to be in breach of UK law, please notify us by emailing eprints@whiterose.ac.uk including the URL of the record and the reason for the withdrawal request.



eprints@whiterose.ac.uk
<https://eprints.whiterose.ac.uk/>

PAPER • OPEN ACCESS

Nanoscale wafer patterning using SPM induced local anodic oxidation in InP substrates

To cite this article: Charlotte Ovenden *et al* 2022 *Semicond. Sci. Technol.* **37** 025001

View the [article online](#) for updates and enhancements.

You may also like

- [Strain evolution of epitaxial tetragonal-like BiFeO₃ thin films on LaAlO₃\(001\) substrates prepared by sputtering and their bulk photovoltaic effect](#)
Seiji Nakashima, Tomohisa Uchida, Kentaro Doi et al.
- [The origin of two-dimensional electron gases at oxide interfaces: insights from theory](#)
N C Bristowe, Philippe Ghosez, P B Littlewood et al.
- [Modulation of electron carrier density at the n-type LaAlO₃/SrTiO₃ interface by water adsorption](#)
Yun Li and Jaejun Yu



IOP | ebooks™

Bringing together innovative digital publishing with leading authors from the global scientific community.

Start exploring the collection—download the first chapter of every title for free.

Nanoscale wafer patterning using SPM induced local anodic oxidation in InP substrates

Charlotte Ovenden^{1,*} , Ian Farrer¹, Maurice S Skolnick² and Jon Heffernan^{1,*}

¹ Department of Electronic and Electrical Engineering, University of Sheffield, S1 3JD Sheffield, United Kingdom

² Department of Physics and Astronomy, University of Sheffield, S3 7RH Sheffield, United Kingdom

E-mail: c.ovenden@sheffield.ac.uk and jon.heffernan@sheffield.ac.uk

Received 28 July 2021, revised 20 October 2021

Accepted for publication 30 November 2021

Published 15 December 2021



CrossMark

Abstract

Atomic force microscopy (AFM) assisted local anodic oxidation (LAO) offers advantages over other semiconductor fabrication techniques as it is a low contamination method. We demonstrate the fabrication of deep and highly reproducible nanohole arrays on InP using LAO. Nanohole and nano-oxide mound radius and depth are controlled independently by altering AFM tip bias and humidity, with a maximum nanohole depth of 15.6 ± 1.2 nm being achieved. Additionally, the effect of tip write speed on oxide line formation is compared for n-type, p-type and semi-insulating substrates, which shows that n-type InP oxidizes at a slower rate than semi-insulated or p-type InP. Finally, we calculate the activation energy for LAO of semi-insulating InP to be 0.4 eV, suggesting the oxidation mechanism is similar to that which occurs during plasma oxidation.

Keywords: nanolithography, atomic force microscopy, semiconductor fabrication

(Some figures may appear in color only in the online journal)

1. Introduction

Nanohole arrays exhibit properties that make them highly useful in optical and electronic applications e.g. facilitation of quantum dot (QD) and surface plasmon coupling [1], and as components in light sensing devices [2]. Particular interest has arisen in a nanohole's ability to nucleate metallic droplets or QDs during epitaxial growth, which is termed site-controlled QD growth [3].

The properties exhibited by QDs make them promising quantum bit (qubit) candidates [4]. A scalable network of

qubits can be created by deterministically positioning large numbers of single QDs within devices, therefore ensuring efficient light coupling of single photon emitters in a quantum circuit architecture [5]. For integration into current commercial communication networks the emission wavelength in such QD photonic systems needs to be in the telecom c-band at 1550 nm [6]. Additionally, each QD must act as a source of indistinguishable photons so that the entangled photon states required for quantum computing can be created. Therefore, the single QD linewidths must be very narrow and ideally close to being Fourier transform limited, where the linewidth of the QD is limited by its lifetime and not broadened by spectral wandering effects [7].

A desirable method of achieving scalable quantum networks is to control the position of QDs during growth, therefore allowing devices to be fabricated around large numbers of deterministically placed emitters. By developing robust and reproducible site-controlled QD growth methods, fabrication

* Authors to whom any correspondence should be addressed.



Original content from this work may be used under the terms of the [Creative Commons Attribution 4.0 licence](https://creativecommons.org/licenses/by/4.0/). Any further distribution of this work must maintain attribution to the author(s) and the title of the work, journal citation and DOI.

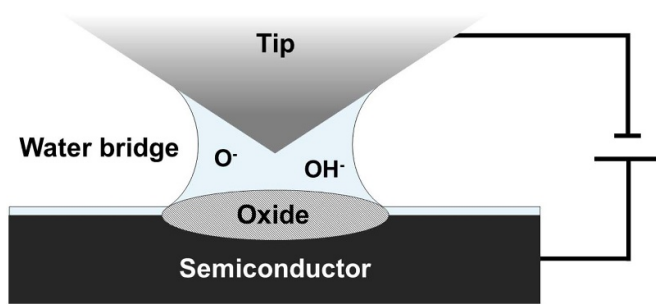


Figure 1. Representation of the local anodic oxidation process, where the applied bias induces the formation of reactive anodic species within the water bridge and facilitates the reaction with the semiconductor to form an oxide that grows above and below the surface.

of scalable qubit networks becomes more readily achievable. To control the QD position, arrays of nanoholes can be fabricated, each acting as an area for preferential nucleation of QD growth. This mechanism occurs via the nanohole reducing the surface chemical potential and providing an increased density of step edges, which reduces energetic requirements for growth and facilitates QD nucleation. Arrays of nanoholes that are highly uniform in shape, pitch and size allow site-controlled QD properties such as position, density, and emission wavelength to be controlled [8]. Processing techniques, such as electron-beam lithography (EBL) with plasma or wet chemical etching (WCE), are commonly used to fabricate the required arrays of nanoholes [9, 10]. However, emission linewidths for site-controlled QDs are generally broader than those for randomly grown QDs, due to a fabrication interface being created that has been exposed to contaminants and process-induced damage [11]. These act as charge traps that lead to spectral wandering of the QD emission wavelength and broadens the linewidths. This broadening can be mitigated by cleaning the surface to as high a degree as possible and by growing the QD as far as practical from the processed surface using an epitaxial buffer layer, which is grown on the processed surface directly prior to QD deposition [12].

An alternative to EBL is the use of local anodic oxidation (LAO), which uses an atomic force microscope (AFM) to assist in the fabrication of nanofeatures [13]. By positioning a biased AFM tip over the surface of a semiconductor, the growth of a nano-scale oxide feature can be established through the formation of a water bridge between the tip and surface (figure 1), where the radius of this water bridge depends on humidity. Reactive O^- and OH^- ions are created within the water bridge, which move under bias towards the semiconductor surface and oxidize it. Therefore, the radius of the water-bridge will directly affect the radius of the feature. The tip voltage affects the depth that these reactive ions can penetrate into the surface and therefore determines the maximum depth that the oxide grows to. The main parameters affecting the dimensions of the oxide formed via LAO and therefore nanohole dimensions are the applied tip bias [14], and humidity [15], in addition to tip-sample distance [16], tip radius [17], and tip writespeed [18].

The oxide features produced via this method can be subsequently removed via WCE or atomic hydrogen cleaning to form arrays of nanoholes [19]. Fabrication of nanoholes via LAO has an advantage over more commonly used lithographic methods in that it does not require the use of organic resist masks that can be difficult to remove properly after processing and are a major source of contamination [20]. Instead, LAO is a maskless, one-step, *ex-situ* process that allows the sample to be transferred immediately into the epitaxy chamber where the nano-oxide features are removed via atomic hydrogen cleaning. Therefore, the method is simple and requires far fewer steps than other fabrication techniques, such as those involving EBL. In previous reports of LAO processing a major drawback was that nanoholes were shallow, which can limit the thickness of a subsequently grown buffer layer within the nanoholes. Linewidth broadening of a QD can be mitigated by growing it on a thick epitaxial buffer, far from the processed interface. Therefore, being limited to use of a thin buffer could negatively impact the linewidth of site-controlled QDs. The site-controlled growth of InAs QDs grown on an InP substrate using nanohole arrays fabricated using LAO has previously been demonstrated [21]. The fabricated nanoholes were 3–4 nm in depth and no epitaxial buffer was deposited on the nanoholes prior to QD growth. The site-controlled QDs emitted at telecom wavelengths, however the reported single QD linewidths of 0.8 meV were much broader than typically required for quantum photonics applications where linewidths of the order 2–20 μeV are required. Further to this, poor homogeneity has also been reported to occur during LAO fabrication, due to field effect diffusion [22]. In addition to LAO being used to form arrays of nanoholes, Komijani *et al* report on the fabrication of oxide lines around a QD on p-type GaAs/AlGaAs heterostructures for electronic transport measurements [23]. They note a difference between spin-orbit and Coulomb interactions in p-type and n-type materials.

In this paper we investigate the application of LAO processing to InP wafers and demonstrate that deep and homogeneous nanoholes can be produced, while maintaining the shape symmetry that is required of nanoholes used to nucleate QDs. We report the effect of humidity and tip voltage on nanohole dimensions and investigate the positioning regularity of the nanoholes within the arrays. We also investigate the influence of tip write speed on formation of oxide lines for n-type, p-type, and semi-insulating substrates.

2. Experimental methods

LAO was investigated in three types of (100) InP substrates; sulfur-doped (n-type), iron doped (semi-insulating) and zinc doped (p-type). The samples underwent an acid dip with 4:1:100 $H_2SO_4/H_2O_2/DI$ water to remove the surface oxide prior to fabrication. All oxidations were then performed using a Bruker Dimension Icon AFM in tapping mode with an OTESPA r3 tip composed of 0.01–0.02 $\Omega\text{ cm}$ silicon with a nominal spring constant of 6 $N\text{ m}^{-1}$ and tip radius of 7 nm. Experiments were carried out in ambient air under a range

of humidities at 25 °C. To produce arrays of oxide mounds the high-resolution tip was positioned at each point for 10 s at an amplitude set-point of 7 mV, where the amplitude set-point controlled the tip-sample distance. A range of negative tip biases are investigated, ranging from -10 V to -22 V. The oxide mounds formed were subsequently removed with the same $\text{H}_2\text{SO}_4/\text{H}_2\text{O}_2$ acid dip, which lead to the formation of arrays of nanoholes. Oxide lines were formed in a similar fashion by scanning the tip across the surface at a constant speed. The depth, height, and diameter information for each nanofeature was extracted from the AFM images using the in-built tool provided by the software Nanoscope Analysis.

3. Results and discussion

Figure 2 shows AFM images for nano-oxide mounds and nanoholes fabricated in arrays on semi-insulating InP at 40% humidity and -18 V tip bias. The oxide mounds shown in figure 2(a) were formed by holding the biased AFM in one position. Figure 2(b) shows the nanoholes subsequently produced by acid etching the nano-oxide mounds. The features are well defined and nanoholes are circular with a mean ellipticity of 0.96; the very slight elongation is present in the $[1-10]$ direction. The mean convexity, which describes the edge roughness of the features, was 0.95. By taking a section through the features they are shown to be conical in shape, therefore suitable for nucleating single QDs [24]. A section through corresponding nano-oxide mounds and nanoholes, shown in figure 2(c), demonstrates that the oxides form above and below the surface.

Figures 3(a) and (b) show nanomound radius and height as a function of tip voltage, measured at the base of each feature. Figures 3(c) and (d) show nanohole radius and depth for the corresponding features. It can be seen that with increasing bias, both the height and radius of the features increase. The increased bias forms a larger electric field around the tip, which increases both the radius of the feature and the penetration depth of the ions. When a constant voltage is applied between the tip and sample for an extended period of time (>0.1 s) space-charge builds up as the oxide grows [25]. This effect leads to some preferential oxide growth in a lateral direction, which in turn causes the increase in the oxide radius. Fabrication of deep nanoholes is achieved by using a high bias in conjunction with the high-resolution AFM tip. The maximum mean depth for an array of nanoholes is 15.6 ± 1.2 nm and a corresponding average radius of 104 nm. This nanohole depth is comparable to EBL fabricated nanoholes, which were previously used to produce low linewidth site-controlled QDs [26]. In contrast, the humidity has a strong influence only over the nanohole radius which again increases with increasing humidity. This is because the humidity affects only the size of the water bridge, not the penetration depth of the ions. This is a critical observation as it allows us to decouple the depth and radius of the nanoholes giving independent control and overcoming the space-charge effects. Table 1 shows a comparison between the nanohole depths used for the site-controlled growth of InAs QDs on GaAs. A range of techniques are

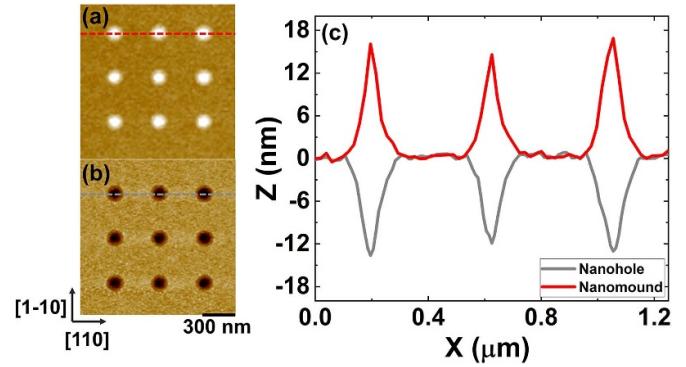


Figure 2. AFM (a) image of fabricated oxide nanomounds, (b) image of nanoholes formed by acid etching of the oxide and (c) cross sections of the features highlighted in (a) and (b). Parameters are -18 V and 40% humidity.

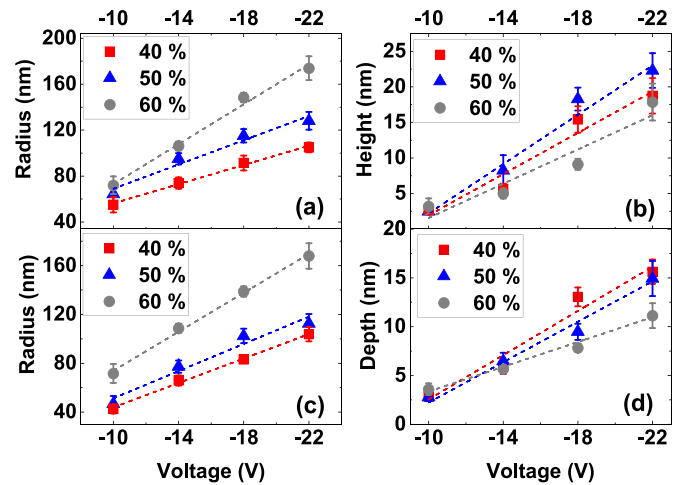


Figure 3. Feature size dependence on voltages of -10 V, -14 V, -18 V and -22 V and humidities of 40%, 50% and 60% shown for (a) nanomound radius (b) nanomound height (c) nanohole radius and (d) nanohole depth. Mean values and standard deviations are calculated from arrays of 25 nano-features for each parameter.

Table 1. The depths of nanoholes fabricated on a GaAs substrate and used to successfully achieve site-controlled growth of InAs QDs compared to the maximum nanohole depths achieved in this work.

Fabrication method	Nanohole depth	Reference
EBL/WCE	18 nm	[9]
EBL/plasma etching	20 nm	[11]
EBL/plasma etching or WCE	15–20 nm	[30]
UV-NIL	15 nm	[31]
LAO	Maximum 15.6 nm	This work

compared, these being EBL with plasma etching, EBL with WCE and ultraviolet nanoimprint lithography (UV-NIL). The nanohole depths achieved in this work are comparable to those used in the literature.

In this study, we observed a low standard deviation (SD) in nanohole radius and depth which is an encouraging result for reducing inhomogeneity in site-controlled QD size, emission wavelength and occupancy [27, 28]. The SD in radius

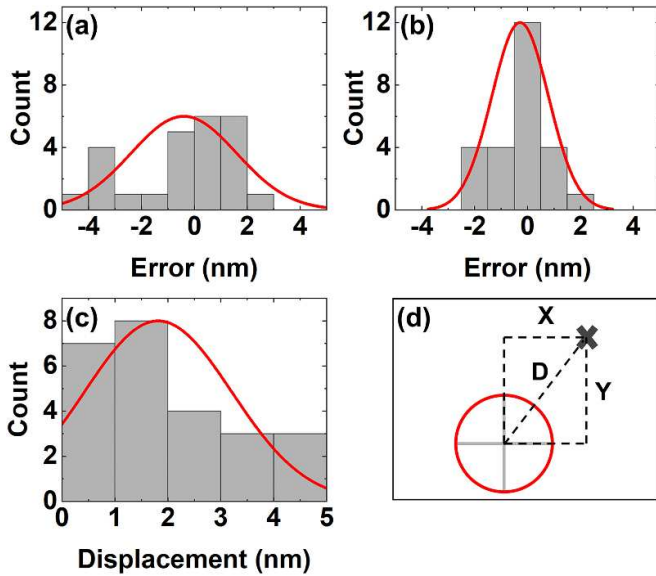


Figure 4. Nanohole positioning regularity compared to an ideal array showing (a) the displacement in X , (b) the displacement in Y , (c) the total displacement (D) and (d) the way the displacements are measured between the nanohole (red circle) and ideal nanohole position (marked with a black cross).

was between 15 and 3 nm, with no trend seen when increasing voltage or humidity. Additionally, the SD in depth was less than 2 nm in all cases and was as low as 0.3 nm for the smallest nanoholes. The deep and reproducible nature of the nanoholes was attributed to the use of an ultra-high resolution tip that has a narrow tip apex. A slight increase in SD of nanohole depth was observed when increasing voltage which is attributed to build up of space-charge and the regime where applied bias has a reduced ability to promote oxide growth [29].

Producing an array of nanoholes that are regularly and controllably positioned is desirable when using the nanoholes for site-controlled QD growth. Because the nanohole controls the growth position of the QD, any irregularity in nanohole positioning will transfer to a site-controlled QD array. Therefore, by fabricating highly regularly posited nanoholes, site-controlled QD positioning is likely to be improved. We measured the deviation in positioning between each nanohole and an ideal array. An example of these measurements, for the array fabricated using a humidity of 40% and tip bias of -22 V is shown in figure 4(a) for the x error, (b) for the y error and (c) for the total displacement (D). The largest displacement between the measured nanohole position and ideal position was 3.8 ± 2.8 nm for the array fabricated using a humidity of 60% and a tip bias of -22 V. No positioning accuracy dependence on fabrication conditions was observed. The measured displacements were very low and would not have negative impact on QD and photonic device coupling or operation.

As well as its potential for use in site-controlled QD formation, LAO has been used to create functional components in heterostructures, where fabrication of oxide lines granted electrical control over a QD [23]. We compare the LAO process

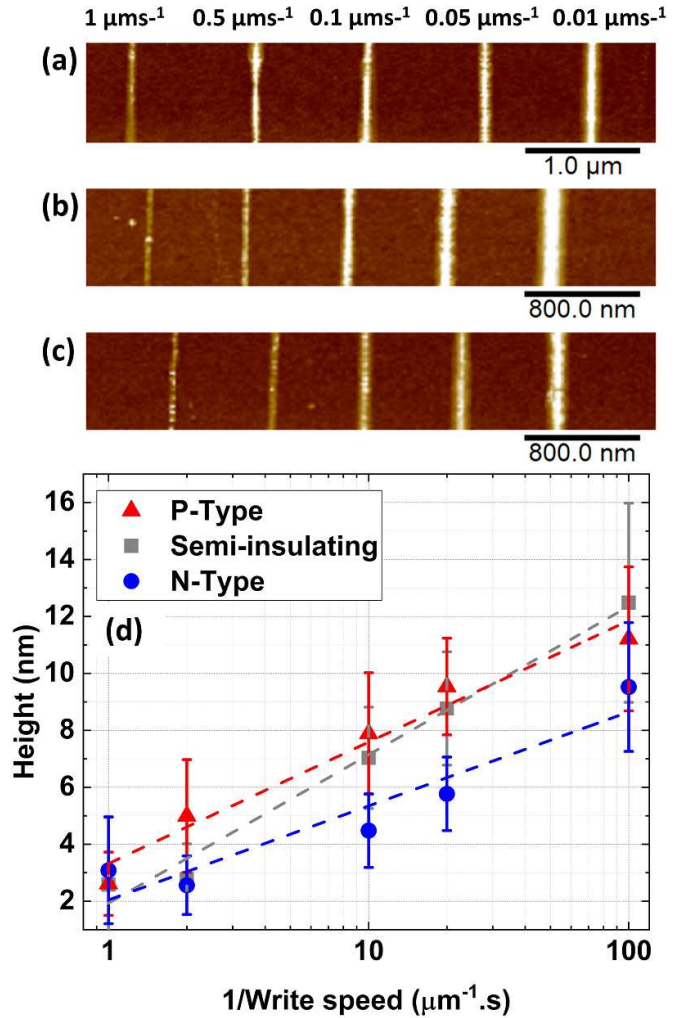


Figure 5. AFM images of oxide lines fabricated by scanning the AFM tip across (a) p-type, (b) semi-insulating and (c) n-type InP at -22 V with tip write speeds of 1, 0.5, 0.1, 0.05, and $0.01 \mu\text{ms}^{-1}$ (left to right) and (d) a plot showing linear relationships between mean height and (log) $1/\text{write speed}$ for each doping type.

on n-type, p-type and semi-insulating InP while varying tip write speed. Figures 5(a)–(c) show AFM images of oxide lines fabricated on p-type, semi-insulating and n-type InP, and figure 5(d) shows the height of the oxide mounds as a function of inverse write speed for each doping type. For all samples, the AFM tip was scanned across the surface in a line with an applied voltage of -22 V at a humidity of 35%. Reducing write speed, which is equivalent to using a longer dwell time, produces a higher oxide growth rate with a linear relationship between height, h and $\log(1/\text{write speed})$ demonstrated for all substrates. This relationship has previously been observed on silicon substrates [32]. The width of the oxide lines increased as tip write speed decreased and there was some difference between the doping types, with the widest oxide lines being formed on semi-insulating InP and the narrowest oxide lines on p-type InP.

The results show that LAO is possible on all InP doping types, however the achievable height of oxide mounds is

affected by doping type, which is explained by the diffusion depth differing for each doping type due to local field effects. For all doping types, tip write speed offers another parameter that allows predictable control of oxide line height. The SD is shown as an error which arises from fluctuation in the oxide height as the tip is scanned across the surface. This fluctuation can be explained via changes in the water bridge as the tip moves across the surface [33]. Dwelling the tip in one position reduced these fluctuations which led to the lower errors observed for the fabricated oxide mounds.

For LAO and oxide growth to occur, anodic ions must overcome an energy barrier to move to a reaction site. This energy is supplied by the tip voltage and affects the height to which an oxide will be able to grow to under certain conditions. The Cabrera–Mott model [34] has been widely used to explain this process [35]. By using an analytical model described by Stiévenard *et al* [36], which was based upon this Cabrera–Mott theory, the activation energy for LAO of a particular material can be calculated via the relationship between oxide height and tip write speed. For silicon, activation energies were calculated to be between 0.1 and 0.4 eV. At tip voltage of -8 V we apply this model to calculate the activation energy for LAO of semi-insulating InP to be 0.4 eV. The same model was applied to GaAs by Cervenka *et al* [37] to produce an activation energy at -8 V of 0.02 eV. The activation energy for thermal oxidation of InP has been reported to be around 2 eV [38], while the activation energy for plasma oxidation was around 0.4 eV [39]. This suggests that the LAO process is more similar to that of plasma oxidation, as is consistent with results shown for LAO if silicon [36]. The result supports the observation that nanoholes that are suitable for the growth of site-controlled QDs that emit in the telecom c-band can be fabricated on InP, as has been demonstrated on GaAs with InAs QDs emitting at 900 nm [40].

4. Conclusions

In conclusion, we have fabricated deep and reproducible nanoholes, with maximum mean depths of 15.6 ± 1.2 nm via LAO on InP. The dimensions of the nanoholes can be controlled via applied tip voltage and humidity so that they are suitable for site-controlled growth of QDs. The deep nature of the nanoholes allows re-growth of thick epitaxial layers and hence assist in reducing QD linewidths. Additionally, the nanoholes are very well defined in shape, which will help maintain QD spectral homogeneity, and are regularly positioned within the array. We also investigated doped substrates and conclude that all doping types are suitable for LAO fabrication. The demonstration of highly uniform nanoholes on InP may further open the way to the site-controlled growth of telecom wavelength QDs.

Data availability statement

The data that support the findings of this study are available upon reasonable request from the authors.

Acknowledgments

This work was supported by EPSRC, Grant No. EP/R03480X/1 and by the InnovateUK project Aquasec. The authors would also like to thank Dominic J Hallett, Chak Lam Chan and Daye Wen for fruitful discussions.

ORCID iD

Charlotte Ovenden  <https://orcid.org/0000-0002-8064-2745>

References

- [1] Brolo G, Kwok S C, Cooper M D, Moffitt M G, Wang C-W, Gordon R, Riordon J and Kavanagh K L 2006 *J. Phys. Chem. B* **110** 8307
- [2] Zhang Z, Zhou J, Wu Y, Xia Z and Qin X 2020 *Appl. Phys. Lett.* **116** 113903
- [3] Sala E, Bollani M, Bietti S, Fedorov A, Esposito L and Sanguinetti S 2014 *J. Vac. Sci. Technol. B* **32** 061206
- [4] Varnava C, Stevenson R M, Nilsson J, Dzurák B, Lucamarini M, Penty R V, Farrer I, Ritchie D A and Shields A J 2016 *npj. Quantum Inf.* **2** 16006
- [5] Lodahl P 2018 *Quantum Sci. Technol.* **3** 013001
- [6] Müller T, Skiba-Szymanska J, Krysta A B, Humer J, Felle M, Anderson M, Stevenson R M, Heffernan J, Ritchie D A and Shields A J 2018 *Nat. Commun.* **8** 62 1
- [7] Uppu R *et al* 2020 *Sci. Adv.* **6** 1–6
- [8] Kaganskiy A, Kreinberg S, Porte X and Reitzenstein S 2019 *Optica* **6** 404
- [9] Jöns K D, Atkinson P, Müller M, Heldmaier M, Ulrich S M, Schmidt O G and Michler P 2013 *Nano Lett.* **13** 126
- [10] Yakes M K *et al* 2013 *Nano Lett.* **13** 4870
- [11] Skiba-Szymanska J *et al* 2011 *Nanotechnology* **22** 065302
- [12] Herranz J, Wewior L, Alén B, Fuster D, González L and González Y 2015 *Nanotechnology* **26** 195301
- [13] Avouris P, Martel R, Hertel T and Sandstrom R 1997 *Appl. Phys. A* **66** S659
- [14] Cha K M, Shibata K, Kamiko M, Yamamoto R and Hirakawa K 2011 *Jpn. J. Appl. Phys.* **50** 120205
- [15] Wang X, Theogene B, Mei H, Zhang J, Huang C, Ren X and Xu M 2019 *Ferroelectrics* **549** 70
- [16] Rius M, Lorenzoni G, Matsui S, Tanemura M and Perez-Murano F 2015 *Beilstein J. Nanotechnol.* **6** 215
- [17] Kozhukhov A S, Scheglov D V, Fedina L I and Latyshev A V 2018 *AIP Adv.* **8** 025113
- [18] Okada Y, Amano S and Kawabe M 1998 *J. Appl. Phys.* **83** 7998
- [19] Martín-Sánchez J, González Y, González L, Tello M, García R, Granados D, García J and Briones F 2005 *J. Cryst. Growth* **284** 313
- [20] Martín-Sánchez J *et al* 2009 *ACS Nano* **3** 1513
- [21] Song H Z, Usuki T, Hirose S, Takemoto K, Nakata Y, Yokoyama N and Sakuma Y 2005 *Appl. Phys. Lett.* **86** 113118
- [22] Tranvouez E, Gendry M, Regreny P and Bremond G 2004 *Superlattices Microstruct.* **36** 325
- [23] Komijani Y, Csontos M, Ihn T, Ensslin K, Reuter D and Wieck A D 2008 *Europhys. Lett.* **84** 57004
- [24] Kumar A, Chen C and Maroudas D 2019 *J. Appl. Phys.* **125** 045303
- [25] Pérez-Murano F, Birkelund K, Morimoto K and Dagata J A 1999 *Appl. Phys. Lett.* **75** 199
- [26] Ryu Y K and Garcia R 2017 *Nanotechnology* **28** 142003

- [27] Mohan A, Gallo P, Felici M, Dwir B, Rudra A, Faist J and Kapon E 2010 *Small* **6** 1268
- [28] Mayer C, Helfrich M and Schaadt D 2013 *Nanoscale Res. Lett.* **8** 504
- [29] Lemeshko S, Gavrilov S, Shevyakov V, Roschin V and Solomatenko R 2001 *Nanotechnology* **12** 273
- [30] Schneider C, Huggenberger A, Gschrey M, Gold P, Rodt S, Forchel A, Reitzenstein S, Höfling S and Kamp M 2012 *Phys. Status Solidi a* **209** 2379
- [31] Cheng C C, Meneou K and Cheng K 2011 *J. Cryst.* **323** 180
- [32] Avouris P, Hertel T and Martel R 1997 *Appl. Phys. Lett.* **71** 285
- [33] Bartošík M, Škoda D, Tomanec O, Kalousek R, Jánký P, Zlamal J, Spousta J, Dub P and Šikola T 2009 *Phys. Rev. B* **79** 195406
- [34] Cabrera N and Mott N F 1949 *Rep. Prog. Phys.* **12** 163–84
- [35] Tseng A A, Lee T-W, Notargiacomo A and Chen T 2009 *J. Micro-Nanolith. MEMS* **8** 043050
- [36] Stiévenard D, Fontaine P A and Dubois E 1997 *Appl. Phys. Lett.* **70** 3272
- [37] Cervenka J, Kalousek R, Bartošík M, Škoda D, Tomanec O and Šikola T 2006 *Appl. Surf. Sci.* **253** 2373
- [38] Yamaguchi M and Ando K 1980 *J. Appl. Phys.* **51** 5007–12
- [39] Sakamoto Y, Sugino T, Ninomiya H, Matsuda K and Shirafuji J 1995 *Jpn. J. Appl. Phys.* **34** 1417
- [40] Herranz J, Gonzalez L, Wewior L, Alén B, Fuster D and González Y 2015 *Cryst. Growth Des.* **15** 666